scientific reports

Check for updates

OPEN

Partial element equivalent circuit modeling of distributed and lumped time-varying dielectric phenomena

Daniele Romano[1], Giuseppe Pettanice[2], Martin Stumpf[3], Ioan E. Lager[4], Jonas Ekman[5], Ondrej Franek[3,7], Roberto Valentini[6], Piergiuseppe Di Marco[6], Fortunato Santucci[6] & Giulio Antonini[1]✉

Time-varying (TV) materials have recently gained considerable attention for their ability to manipulate electromagnetic (EM) waves and improve the performance beyond the limits of conventional time-invariant materials. In addition, distributed TV capacitors are becoming more attractive to achieve particular effects. This work presents a systematic approach to modeling TV dielectrics by incorporating TV capacitors in the framework of the partial element equivalent circuit (PEEC) method. Thus, the standard formulation of the PEEC method is modified to include TV dielectrics and lumped elements for general 3D geometries directly in the time domain (TD). It is shown that this is possible through TV capacitances and voltage-controlled current sources. Four numerical examples validate the proposed approach.

There is a renewed interest in "temporal materials" based on time-varying (TV) constitutive parameters. Recent advancements in material synthesis have allowed the development of electromagnetic (EM) systems where the dielectric permittivity can be controlled externally. This feature suggests translating to time concepts and tools introduced in conventional (spatially modulated) materials[1].

This topic is not new despite the recent interest in employing time-modulation techniques for engineering the EM response. Indeed, some pioneering works have been published starting in the 1950s focusing on the EM propagation through one-dimensional domains with TV permittivity[2–4] and networks with TV lumped elements[5,6]. For example, a comprehensive literature review of EM systems and circuits with TV parameters can be found in[7,8]. More recently, an elegant method to handle circuits with TV components has been presented in[9] but, still, it becomes computationally very expensive when the number of TV elements increases since the size of the problem scales linearly with the number of harmonics. TV components for enhancing the wireless transfer of power and information are also considered in[10]. The use of frequency-domain (FD) techniques results in the solution of a large system of equations, even in the case of circuits involving only one lumped TV component. It becomes unfeasible for problems involving many TV elements.

Tunable components using bulk-distributed properties directly rather than semi-lumped active components have been presented in[11,12]. At the same time, nonreciprocal antennas and circulators are described in[13], and[14,15] respectively.

The literature study reveals that while several methods can handle dielectrics with TV permittivity, most resort to a time-to-frequency transformation. The FD analysis can help to reveal how TV EM systems can surpass the performance limitations of conventional devices (e.g., the Bode-Fano limit). Still, it may not render a proper way to solve a *space-time* problem.

In particular, TV dielectrics have been found of interest in various high-power and optical applications; e.g., space-time modulation of permittivity has been recently explored as a mechanism for designing non-reciprocal

[1]Dipartimento di Ingegneria Industriale e dell'Informazione e di Economia, Università degli Studi dell'Aquila, L'Aquila 67100, Italy. [2]CNRS, CentraleSupélec, Laboratoire des Signaux et Systèmes, Université Paris-Saclay, Gif-sur-Yvette 91190, France. [3]FEEC, Department of Radio Electronics, Lerch Lab of EM Research, Brno University of Technology, Brno 616 00, Czech Republic. [4]Faculty of Electrical Engineering, Mathematics and Computer Science, Delft University of Technology, Delft 2628 CD, The Netherlands. [5]Luleå University of Technology, Luleå, Sweden. [6]Dipartimento di Ingegneria e Scienze dell'Informazione e Matematica, Università degli Studi dell'Aquila, L'Aquila 67100, Italy. [7]Department of Electronic Systems, APMS Section, Aalborg University, Aalborg 9220, Denmark. ✉email: giulio.antonini@univaq.it

devices[16]. Because of frequency mixing introduced by the temporal change in the permittivity, traditional FD analysis techniques are less suitable for use, while a direct integration of Maxwell's equations in the time domain (TD) is the natural approach for this class of problems. Indeed, a rigorous FD method to study wave propagation in inhomogeneous and homogeneous TV dielectric media has been presented in[17]. Here, to perform the study completely in FD, two angular frequencies are introduced: the first frequency argument is related to the temporal nonlocality (or temporal dispersion), and the second argument is associated with the observation time. This is necessary because the TD susceptibility kernel for such a medium is a function of two different time variables. A purely TD approach seems better suited to overcome this issue.

Another possibility that is being explored is to use distributed TV lumped elements to achieve particular performance, as occurs in spatially discrete traveling-wave-modulated circuit networks[18,19] where a transmission line is loaded with spatially discrete traveling-wave-modulated capacitors. Further relevant works on the electromagnetics of TV media recently occurred in the literature: potentialities of TV interfaces have been studied[20–22], for instance. Transmission lines with TV wave speed have been considered in[23]. Moreover, the pulsed EM plane-wave interaction with TV thin high-contrast layers has been presented in[24–26]. Pulsed-source radiated EM field in a homogeneous, isotropic, lossless medium with constant wave impedance/admittance but with TV wave speed has been investigated in[27].

From this literature search, it can be claimed that, despite the growing interest in EM problems in which TV media and TV discrete components with assigned laws are present, the literature on this topic is dominantly limited to particular semi-infinite, 1-D or 2-D geometric structures, with particular modulations of lumped elements, typically the sinusoidal one.

Among techniques developed for analyzing transient EM field interactions with time-dependent materials, TD integral equation (TD-IE) solvers[28,29] offer several advantages over their differential equation counterparts, including finite-difference TD methods[30,31]. In[32], it is presented an envelope-tracking solution of the volume electric-field integral equation (V-EFIE) pertinent to the analysis of wave propagation through spatiotemporally modulated lossy dielectrics, where the material properties vary much slower than the fields. In[33], an explicit marching on-in-time (MOT) scheme for solving the TD EFIE enforced on volumes with TV dielectric permittivity is proposed.

Another integral equation-based approach is represented by the partial element equivalent circuit (PEEC)[34,35]. Its distinctive feature is that it provides a circuit interpretation of EM phenomena for both TD and FD domains. Over the years, several methods for analyzing PEEC models in the time and frequency domains have been proposed[35] and have been further advanced in recent years[36–41].

Equivalent circuit models for ideal dielectrics have been proposed in[42], while equivalent circuits of dispersive and lossy dielectrics have been presented in[43] and[44], respectively. Valuable models of finite-size dielectrics have been recently proposed in[45,46]. Some preliminary results on the modeling of TV dielectrics through the PEEC method have been presented in[47].

This work aims to present a systematic modeling of TV dielectrics in the framework of the 3D PEEC method, along with the incorporation of general TV lumped capacitors. Firstly, a detailed derivation of the contrast-source formulation for TV dielectrics is presented; secondly, based on the contrast-source formulation, TV dielectrics are incorporated in the PEEC formulation based on the volume integral form of Maxwell's equations. It is shown that equivalent circuits that consist of TV capacitances and voltage-controlled current sources can be derived for both lossless and lossy TV dielectrics. The advantage of the proposed approach over the method of moments (MoM)-oriented formulations resides in the circuit interpretation of the phenomena resulting in TV capacitances and controlled sources. It is also true that the same approach can be used along with MoM. It is to be remarked that the proposed approach is a pure TD technique that avoids switching back and forth to the FD, which is not convenient for TV materials and lumped elements. Compared with FDTD[31] and FEM[48] methods, the proposed PEEC modeling of TV dielectrics offers a full-wave circuit interpretation that naturally integrates lumped elements and time-varying materials (e.g., through time-varying capacitors and controlled sources), is suitable for SPICE co-simulation, avoids volumetric meshes of the background medium and the need to enforce absorbing boundary conditions, thus reducing the degrees of freedom, while preserving correct propagation and radiation.

The proposed method is validated through four pertinent examples.

Contrast-source formulation for time-varying dielectrics

In the following, we assume the constitutive relations in a linear, relaxation-free isotropic TV medium exhibiting a TV electrical permittivity $\varepsilon(t)$ and time-independent conductivity σ and magnetic permeability μ_0. They read:

$$J(r,t) = \sigma E(r,t), \tag{1a}$$

$$B(r,t) = \mu_0 H(r,t), \tag{1b}$$

$$D(r,t) = \varepsilon(t) E(r,t). \tag{1c}$$

Let $\{E, H, D, B, J\}(r,t)$ represent the EM fields that solve Maxwell's equations under an assigned excitation:

$$\nabla \times E(r,t) = -\partial_t B(r,t), \tag{2a}$$

$$\nabla \times H(r,t) = J(r,t) + \partial_t D(r,t), \tag{2b}$$

where ∂_t denotes the time differentiation operator. In addition to the curl Maxwell's equations (2), divergence equations must also be considered. For an isotropic TV medium described by $\{\sigma, \mu_0, \varepsilon(t)\}$, they read:

$$\nabla \cdot B(r,t) = 0, \tag{3a}$$

$$\nabla \cdot D(r,t) = \nabla \cdot [\varepsilon(t) E(r,t)] = q^F(r,t), \tag{3b}$$

where $q^F(r,t)$ denotes the free electric charge density.

Equation (2b) can be rewritten as

$$\nabla \times H(r,t) = J(r,t) + \partial_t \left\{ \left[\varepsilon(t) - \varepsilon_0 \right] E(r,t) \right\} + \varepsilon_0 \partial_t E(r,t). \tag{4}$$

By defining the equivalent contrast electric-current volume density as

$$J_{eq}(r,t) = J(r,t) + \partial_t \left\{ \left[\varepsilon(t) - \varepsilon_0 \right] E(r,t) \right\}, \tag{5}$$

equation (4) can be reformulated as

$$\nabla \times H(r,t) = J_{eq}(r,t) + \varepsilon_0 \partial_t E(r,t). \tag{6}$$

The magnetic vector potential $A(r,t)$ generated by $J_{eq}(r,t)$ is given as

$$A(r,t) = \frac{\mu_0}{4\pi} \int_{V'} \frac{J_{eq}(r',t')}{|r-r'|} dV'. \tag{7}$$

In equation (7), t' represents the time at which the equivalent current density J_{eq} acts as the source of the vector potential A, while t denotes the observation time. These two instants are related by:

$$t' = t - |r - r'|/c_0, \tag{8}$$

where c_0 is the speed of light in the vacuum, $c_0 = 1/\sqrt{\mu_0 \varepsilon_0}$. It is well-known that the electric field at position r, at time t, reads:

$$E(r,t) = E^{inc}(r,t) - \partial_t A(r,t) - \nabla \Phi(r,t). \tag{9}$$

In addition to the EFIE, the conservation of charge has to be enforced through the continuity equation. The divergence of equation (6) gives

$$\nabla \cdot J_{eq}(r,t) = -\varepsilon_0 \partial_t \nabla \cdot E. \tag{10}$$

Since the PEEC method is based on the volume equivalence principle, currents and charge densities are assumed to radiate in the free space. This implies

$$\nabla \cdot E(r,t) = \frac{q^F(r,t) + q^B(r,t)}{\varepsilon_0}, \tag{11}$$

where $q^B(r,t)$ is the bound charge due to dielectric polarization[42]. Hence, equation (10) can be rewritten as

$$\nabla \cdot J_{eq}(r,t) = -\partial_t \left[q^F(r,t) + q^B(r,t) \right] = -\partial_t q(r,t). \tag{12}$$

In the following, we assume that the free and bound charges are located only on the surface of conductors, dielectrics, and magnetic materials. Thus, in their interior regions, the continuity equation (10) becomes:

$$\nabla \cdot J_{eq}(r,t) = 0, \tag{13}$$

while on the surfaces, using the surface divergence operator, we have:

$$\left[J_{eq}^+(r,t) - J_{eq}^-(r,t) \right] \cdot \hat{n} = -\partial_t q(r,t), \tag{14}$$

where $\hat{n}$ is the outward normal to the surface S, and the superscripts + and - indicate the two sides of the surface, respectively, and $q(r,t)$ is the total surface charge density. The application of the Gauss theorem to equations (13) and (14) leads to interpreting them as Kirchhoff current law enforced at a node located at point r at time t.

Finally, since the total charge $q(r,t)$ radiate in the free space, the electric scalar potential $\Phi(r,t)$ can be obtained as

$$\Phi(r,t) = \frac{1}{4\pi\varepsilon_0} \int_S \frac{q(r',t')}{|r-r'|} dS'. \tag{15}$$

The equivalent sources can be further expressed as:

$$J_{eq}(r,t) = J(r,t) + \left[\varepsilon(t) - \varepsilon_0\right]\partial_t E(r,t) + E(r,t)\partial_t \varepsilon(t). \tag{16}$$

The above equation can be particularized by considering two distinct classes of (TV) dielectrics:

- lossless TV dielectric $\{\sigma = 0, \varepsilon(t), \mu = \mu_0\}$

$$J_{eq}(r,t) = \left[\varepsilon(t) - \varepsilon_0\right]\partial_t E(r,t) + E(r,t)\partial_t \varepsilon(t), \tag{17}$$

- lossy TV dielectric $\{\sigma, \varepsilon(t), \mu = \mu_0\}$

$$J_{eq}(r,t) = \sigma E(r,t) + \left[\varepsilon(t) - \varepsilon_0\right]\partial_t E(r,t) + E(r,t)\partial_t \varepsilon(t). \tag{18}$$

PEEC formulation for time-varying dielectric phenomena

To derive a PEEC-based representation of TV dielectric phenomena, equations (7) and (15) are employed to reformulate equations (9), (13), and (14) into equivalent circuit equations. This transformation is carried out through a two-step procedure:

1. The unknown quantities $J_{eq}(r,t)$ and $q(r,t)$ are expanded in a series form as:

$$J_{eq}(r,t) \cong \sum_{n=1}^{N_v} b_n(r)\, I_n(t), \tag{19a}$$

$$q(r,t) \cong \sum_{m=1}^{N_s} p_m(r)\, Q_m(t), \tag{19b}$$

where $b_n(r) \in \mathscr{R}^3$ and $p_m(r) \in \mathcal{R}$ are the spatial basis functions, while $I_n(t)$ and $Q_m(t)$ are the basis function weights that must be determined at each time sample, N_v and N_s represent the number of elementary volumetric and surface sub-regions, respectively;

2. Upon substitution of (19) in (7), (15), (9), (13) and (14), Galerkin's testing or weighting process[49] is adopted by enforcing the residuals of equations (9) and (15) to be orthogonal to a set of weighting functions, which are identical to the basis functions. To this aim, two inner products are defined as:

$$\langle f(r), b_i(r)\rangle = \int_{V_i} f(r)\cdot b_i(r)\, dV_i, \tag{20a}$$

$$\langle g(r), p_j(r)\rangle = \int_{S_j} g(r)\cdot p_j(r)\, dS_j, \tag{20b}$$

with $i = 1, \cdots, N_v$, and $j = 1, \cdots, N_s$.

Although various types of basis functions may be employed to expand the current and charge densities, in this work, we focus on the case of orthogonal geometries. Specifically, we assume that the volumes and surfaces of the structure are discretized into N_v elementary parallelepipeds and N_s rectangular patches, respectively. These elements are assumed to be electrically small with respect to the wavelength corresponding to the highest frequency of interest. Accordingly, piecewise constant basis functions are adopted throughout the following analysis.

Let us denote by ℓ_n and a_n the length and the cross-section of an elementary parallelepiped V_n, respectively. The basis functions used to expand the current density $J(r,t)$ are chosen as:

$$b_n(r) = \begin{cases} \frac{\hat{u}_n}{a_n} & \text{if } r \in V_n \\ 0 & \text{otherwise} \end{cases}, \tag{21}$$

where $\hat{u}_n$ is the unit vector indicating the current orientation in volume V_n. With such a choice of the basis function, the corresponding weight represents the current flowing in the volume V_n with orientation $\hat{u}_n$.

Let A_m be the area of the surface of the rectangular patch S_m. The basis functions used to expand the charge density $q(r,t)$ are chosen as:

$$p_m(r) = \begin{cases} \frac{1}{A_m} & \text{if } r \in S_m \\ 0 & \text{otherwise} \end{cases} \tag{22}$$

With such a choice of the basis function, the corresponding weight Q_m represents the charge on patch m.

Figure 1 describes the overall process of derivation of the PEEC method. In particular, it shows the block diagram of the PEEC workflow from the electromagnetic to the circuit domain: starting from geometry and

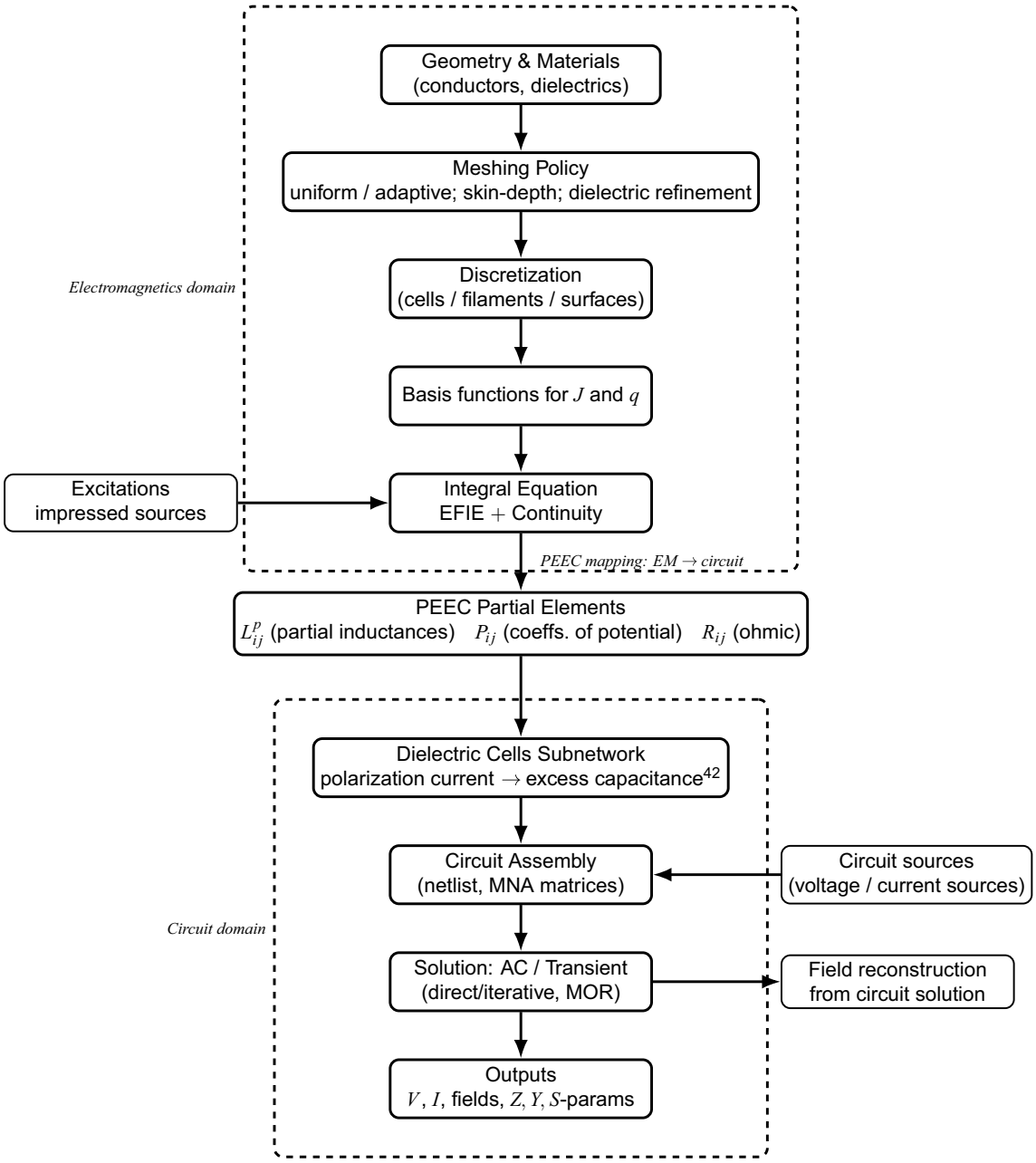

Fig. 1. Block diagram of the PEEC workflow from the electromagnetic to the circuit domain.

materials, meshing and discretization define the basis functions for J and q, on which EFIE and charge continuity are enforced; the mapping yields the partial elements, e.g., partial inductances, coefficients of potential, and resistances. Lossless and lossy/dispersive dielectrics can be incorporated as described in[42,43]. The resulting circuit is assembled in the modified nodal analysis (MNA)[50] and solved in the frequency or time domain (optionally with reduced order models[51–55]). Outputs include voltages, currents, fields, and port parameters (Z, Y, S parameters). Excitations can be introduced either in the EM or the circuit domain; a field-reconstruction block enables back-mapping of fields.

The following sections present PEEC-based models for TV dielectrics (lossless and lossy) and for time-varying lumped capacitors.

Time-varying lossless dielectrics

For a TV lossless dielectric, the equivalent current density at a point r and at time t (17) can be rewritten as

$$J_{eq}(r,t) = \left[\varepsilon(t) - \varepsilon_0\right]\partial_t E(r,t) + E(r,t)\partial_t \varepsilon(t), \tag{23}$$

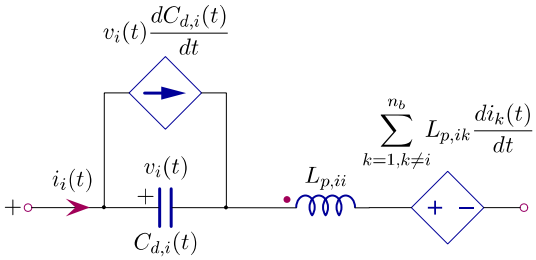

Fig. 2. Equivalent circuit for a lossless TV dielectric cell.

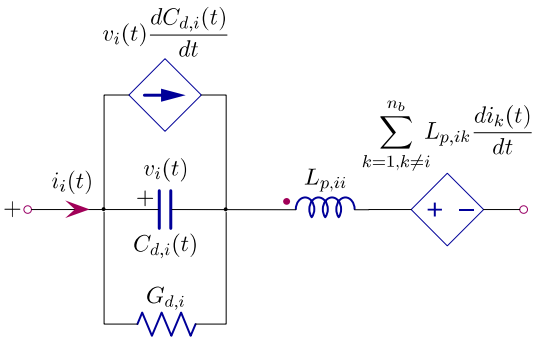

Fig. 3. Equivalent circuit for a lossy TV dielectric cell.

Also in this case, using the expansion (19a) and applying the inner product (20a) for the i-th elementary volume, allows to obtain the circuit interpretation of equation (23):

$$i_i(t) = C_{d,i}(t)\frac{dv_i(t)}{dt} + v_i(t)\frac{dC_{d,i}(t)}{dt}, \tag{24}$$

where $C_{d,i}(t)$ is the TV excess capacitance[42] and $v_i(t)$ is the voltage drop across the i-th elementary volume. The corresponding equivalent circuit is described in Fig. 2. It consists of the TV excess capacitance $C_{d,i}(t)$ in parallel with a voltage-controlled current source proportional to the time derivative of the excess capacitance $C_{d,i}(t)$.

Time-varying lossy dielectrics

In the case of TV lossy dielectrics, the equivalent current density at a point r and at time t is given by (18). Following the same steps as before, we obtain

$$i_i(t) = G_{d,i}v_i(t) + C_{d,i}(t)\frac{dv_i(t)}{dt} + v_i(t)\frac{dC_{d,i}(t)}{dt}, \tag{25}$$

where $G_{d,i}$ is the conductance of the i-th elementary volume. The corresponding equivalent circuit is shown in Fig. 3. Hence, the additional conductance $G_{d,i}$ is placed in parallel to the equivalent circuit of the lossless case.

Time-varying lumped capacitors

TV lumped capacitors can also be used to overcome the performance of time-invariant capacitors. In this case, the current through the time-varying capacitor C_{lc} is

$$i_{lc,i}(t) = \frac{dq}{dt} = C_{lc,i}(t)\frac{dv_{lc,i}(t)}{dt} + v_{lc,i}(t)\frac{dC_{lc,i}(t)}{dt}. \tag{26}$$

The corresponding circuit synthesis is shown in Fig. 4.

TV capacitors can be stamped in the Modified Nodal Analysis (MNA) form[50], as reported in the next section.

Time domain PEEC formulation

In the previous section, it has been shown that TV dielectrics and lumped capacitors can be included in PEEC models in terms of TV capacitances and voltage-controlled current sources, accounting for the time derivative of the TV permittivity or capacitance. This results in the equivalent circuits in Figs. 2, 3 and 4. Hence, they impact only the Kirchhoff voltage (KVL) that has to be enforced on the PEEC circuit. It is also to be remarked that such circuits are fully compatible with Spice-like tools[56–58], thus making it possible to integrate the PEEC model with other linear and non-linear elements as available in circuit libraries.

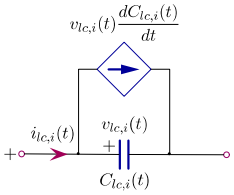

Fig. 4. Equivalent circuit for a TV capacitor.

In the following, the TD PEEC formulation described in[59] is adopted, by taking equations (24), (25) and (26) into account. The MNA form of the adopted equations is:

$$\mathrm{C}(t)\frac{d\mathrm{x}(t)}{dt} = -\mathrm{G}(t)\mathrm{x}(t) + \mathrm{Bu}(t), \tag{27}$$

with the unknown vector being

$$\mathrm{x}(t) = [\mathrm{i}(t) \quad \phi_{sr}(t) \quad \phi_i(t) \quad \mathrm{v}_d(t) \quad \mathrm{q}_s(t)]^T \in \Re^{n_u \times 1}, \tag{28}$$

where $\mathrm{i}(t)$ are the branch currents, $\phi_{sr}(t)$ are the scalar potentials for surface nodes, $\phi_i(t)$ are the scalar potentials for internal nodes, $\mathrm{v}_d(t)$ are the excess capacitance voltages for dielectric branches $\mathrm{q}_s(t)$ are the surface charges, and n_u is the total number of unknowns. The state-space matrices $\mathrm{C}(t)$, $\mathrm{G}(t)$ and B retain the same structural form as in the time-invariant case[60], but now include entries that are explicitly time-varying. They are given by:

$$\mathrm{C}(t) = \begin{bmatrix} \underset{n_b\times n_b}{\mathrm{L}_p(t)*} & \underset{n_b\times n_{ns}}{0} & \underset{n_b\times n_{ni}}{0} & \underset{n_b\times n_{bd}}{0} & \underset{n_b\times n_p}{0} \\ \underset{n_{ns}\times n_b}{0} & \underset{n_{ns}\times n_{ns}}{\mathrm{C}_{lc}(t)} & \underset{n_{ns}\times n_{ni}}{0} & \underset{n_{ns}\times n_{bd}}{0} & \underset{n_{ns}\times n_p}{\mathrm{M}^T} \\ \underset{n_{ni}\times n_b}{0} & \underset{n_{ni}\times n_{ns}}{0} & \underset{n_{ni}\times n_{ni}}{0} & \underset{n_{ni}\times n_{bd}}{0} & \underset{n_{ni}\times n_p}{0} \\ \underset{n_{bd}\times n_b}{0} & \underset{n_{bd}\times n_{ns}}{0} & \underset{n_{bd}\times n_{ni}}{0} & \underset{n_{bd}\times n_{bd}}{\mathrm{C}_d(t)} & \underset{n_{bd}\times n_p}{0} \\ \underset{n_p\times n_b}{0} & \underset{n_p\times n_{ns}}{0} & \underset{n_p\times n_{ni}}{0} & \underset{n_p\times n_{bd}}{0} & \underset{n_p\times n_p}{0} \end{bmatrix}, \tag{29}$$

$$\mathrm{G}(t) = \begin{bmatrix} \underset{n_b\times n_b}{\mathrm{R}} & \underset{n_b\times n_{ns}}{\mathrm{A}_s} & \underset{n_b\times n_{ni}}{\mathrm{A}_i} & \underset{n_b\times n_{bd}}{\boldsymbol{\Gamma}} & \underset{n_b\times n_p}{0} \\ \underset{n_{ns}\times n_b}{-\mathrm{A}_s^T} & \underset{n_{ns}\times n_{ns}}{\mathrm{G}_{le}(t)} & \underset{n_{ns}\times n_{ni}}{0} & \underset{n_{ns}\times n_{bd}}{0} & \underset{n_{ns}\times n_p}{0} \\ \underset{n_{ni}\times n_b}{-\mathrm{A}_i^T} & \underset{n_{ni}\times n_{ns}}{0} & \underset{n_{ni}\times n_{ni}}{0} & \underset{n_{ni}\times n_{bd}}{0} & \underset{n_{ni}\times n_p}{0} \\ \underset{n_{bd}\times n_b}{-\boldsymbol{\Gamma}^T} & \underset{n_{bd}\times n_{ns}}{0} & \underset{n_{bd}\times n_{ni}}{0} & \underset{n_{bd}\times n_{bd}}{\mathrm{G}_d(t)} & \underset{n_{bd}\times n_p}{0} \\ \underset{n_p\times n_b}{0} & \underset{n_p\times n_{ns}}{-\mathrm{M}} & \underset{n_p\times n_{ni}}{0} & \underset{n_p\times n_{bd}}{0} & \underset{n_p\times n_p}{\mathrm{P}(t)*} \end{bmatrix}, \tag{30}$$

where $\mathrm{G}_d(t) = \mathrm{G}_d + \frac{d}{dt}\mathrm{C}_d(t)$, $\mathrm{G}_{le}(t) = \mathrm{G}_{lr} + \frac{d}{dt}\mathrm{C}_{lc}(t)$, G_{lr} being the matrix including time-invariant lumped resistances and

$$\mathrm{B} = \begin{bmatrix} \underset{n_b\times n_b}{\mathscr{I}} & \underset{n_b\times n_{ns}}{0} \\ \underset{n_{ns}\times n_b}{0} & \underset{n_{ns}\times n_{ns}}{\mathscr{I}} \\ \underset{n_{ni}\times n_b}{0} & \underset{n_{ni}\times n_{ns}}{0} \\ \underset{n_{bd}\times n_b}{0} & \underset{n_{bd}\times n_{ns}}{0} \\ \underset{n_p\times n_b}{0} & \underset{n_p\times n_{ns}}{0} \end{bmatrix}, \tag{31}$$

where n_b, n_{ns}, n_{ni}, n_{bd} and n_p represent the cardinality of branches, surface nodes, internal nodes, dielectric cells, and surface cells, respectively. The time-dependent partial inductance matrix $\mathrm{L}_p(t)$ and the coefficient of potential matrix $\mathrm{P}(t)$, which describe the magnetic and electric field coupling in the background medium, can be written as:

$$\mathrm{L}_p(t) = \mathrm{L}_p^{(dl)}\delta(t) + \sum_{i=1}^{N_{L_p}} \mathrm{L}_p^{(d)}\delta(t - \tau_{cc,i}), \tag{32a}$$

$$\mathrm{P}(t) = \mathrm{P}^{(dl)}\delta(t) + \sum_{q=1}^{N_P} \mathrm{P}^{(d)}\delta(t - \tau_{cc,q}), \tag{32b}$$

where *dl* and *d* stand for delay-less and delayed components, respectively; N_{L_p} is the number of not-negligible delays between elementary volumes, while N_P is the number of not-negligible delays between elementary surfaces; $\tau_{cc,i} = R_{cc,i}/c_0, i = 1, \cdots, N_{L_p}$ and $\tau_{cc,q} = R_{cc,q}/c_0$, $q = 1, \cdots, N_P$ denote the delays between the centers, identified by $R_{cc,i}$ and $R_{cc,q}$ respectively, of the spatial supports of the basis functions of currents and charges; c_0 is the speed of the light in the background medium. The symbol $*$ denotes the convolution operator. Furthermore, $\mathrm{C}_d(t)$ is the TV excess capacitance matrix, $\mathrm{G}_d(t)$ is the matrix accounting for the dielectric conductive losses and the time derivative of the TV excess capacitance matrix, R is the branches resistance matrix, A_s is the incidence matrix for the surface nodes, A_i is the incidence matrix for the internal nodes, $\mathbf{\Gamma}$ is the dielectric region selection matrix, M is the surface-to-node reduction matrix and G_{le} is the load conductance matrix (assuming for simplicity of notation that only resistive lumped elements are connected to the PEEC model).

The source vector $\mathrm{u}(t)$ is:

$$\mathrm{u} = \begin{bmatrix} \mathrm{v}_s(t) \\ \mathrm{i}_s(t) \end{bmatrix}, \tag{33}$$

where $\mathrm{v}_s(t)$ and $\mathrm{i}_s(t)$ are the voltage and current sources applied to branches and nodes, respectively. Vector $\mathrm{v}_s(t)$ includes the voltages induced by external incident fields[61].

It is to be remarked that the partial inductances L_p and the coefficients of potential P are not affected by the TV behavior of dielectrics because they describe the magnetic and electric field coupling in the background medium, typically the free space. Time variation of the permittivity is reflected only in the $\mathrm{C}_d(t)$ and $\mathrm{G}_d(t)$ matrices that describe local dielectric polarization phenomena. The solver obtained using the partial inductance matrix $\mathrm{L}_p(t)$ and the coefficient of potential matrix $\mathrm{P}(t)$, as defined in equation (32), is the one with delay, hereafter referred to as $PEEC - DEL$. If, starting from this, the propagation delays are neglected, the quasi-static version is obtained, hereafter referred to as $PEEC - QS$.

Time-domain solver

In this sub-section, a simple algorithm for the computation of the time-domain solution is given. In particular, it is summarized by the procedure TIME-DOMAIN-SOLVER given in Fig. 5.

At line 1, the $k-$th time instant (0 initial time), the vector of unknowns X and its time derivative X' are initialized. From line 2 to line 9, the solution X_k is iteratively computed for each time sample *k*. In particular, at line 3 the *k*-th time instant is increased by the time step size *h*. At lines 4 and 5, the matrices $\mathrm{C}_{lc}(t_k)$, $\mathrm{C}_d(t_k)$, $\mathrm{G}_{le}(t_k)$ and $\mathrm{G}_d(t_k)$ are updated by exploiting equations (25) and (26). As consequence, matrices $\mathrm{C}(t_k)$ and $\mathrm{G}(t_k)$ of equations (29) and (30), respectively, needs to be updated. At line 6, the source vector u_k is updated including the voltage and current sources at the time instant t_k and including the contribution of the delays for matrices L_p and P (32). At line 7, the linear system $\left[h\mathrm{C}(t_k) + \mathrm{G}(t_k)\right]\mathrm{X}_k = \mathrm{u}_k$ is solved to compute the solution X_k and, finally, at line 8, its time derivative X'_k is computed.

GMRES iterative solver

Since the coefficient matrix $\left[h\mathrm{C}(t_k) + \mathrm{G}(t_k)\right]\mathrm{X}_k = \mathrm{u}_k$ must be updated at each time instant t_k, employing a direct solver, such as LU decomposition or explicit matrix inversion, becomes computationally prohibitive even for problems of moderate size. Therefore, an iterative solver, such as the Generalized Minimal Residual (GMRES) algorithm[62], is necessary. In terms of iterative solvers, a well-conditioned system matrix corresponds to a low number of iterations for convergence. First of all, the system $\left[h\mathrm{C}(t_k) + \mathrm{G}(t_k)\right]\mathrm{X}_k = \mathrm{u}_k$ is typically

Procedure: TIME-DOMAIN-SOLVER
Output: **X**

1 initialize $t_k = 0$, $\mathbf{X} = \mathbf{0}$, $\mathbf{X}' = \mathbf{0}$
2 **for** each time sample **do**
3 $t_k = t_k + h$
4 update $\mathbf{C}_{lc}(t_k)$ in (29) and $\mathbf{G}_{le}(t_k)$ in (30)
5 update $\mathbf{C}_d(t_k)$ in (29) and $\mathbf{G}_d(t_k)$ in (30)
6 compute $\mathbf{u}_k$ at time t_k
7 solve $\left[h\mathbf{C}(t_k) + \mathbf{G}(t_k)\right]\mathbf{X}_k = \mathbf{u}_k$
8 compute $\mathbf{X}'_k$
9 **end for**

Fig. 5. Pseudocode of procedure TIME-DOMAIN-SOLVER.

Scalar electric potential	Voltage	Current	Charge	P_s	C_d	R	L_p	Time
V	V	mA	pC	pF^{-1}	pF	kΩ	μH	ns

Table 1. Scaled Units.

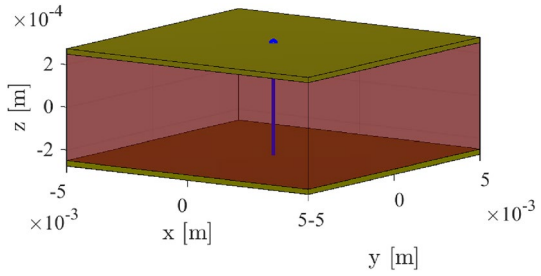

Fig. 6. Parallel plate capacitor.

ill-conditioned because charges are usually much smaller than currents and voltages. To mitigate this problem, scaling can be adopted. The units of the electrical quantities are changed consistently as shown in Table 1.

Furthermore, it has been found effective to construct the preconditioner as the inverse of the matrix $\left[h\hat{\mathrm{C}}(t_k)+\hat{\mathrm{G}}(t_k)\right]$, where $\hat{\mathrm{C}}(t_k)$ and $\hat{\mathrm{G}}(t_k)$ are built in the same manner as $\mathrm{C}(t_k)$ and $\mathrm{G}(t_k)$ in equations (29) and (30), respectively. However, the dense matrices L_p and P are replaced with the diagonal matrices $\hat{\mathrm{L}}_p$ and $\hat{\mathrm{P}}$, which retain only the diagonal elements as non-zero entries. Since $\left[h\hat{\mathrm{C}}(t_k)+\hat{\mathrm{G}}(t_k)\right]$ is very sparse, its inversion can be easily performed by resorting to the sparse multifrontal LU factorization[63]. Finally, the GMRES method was implemented with a custom block-by-block redefinition of the matrix–vector products and manual block-wise preconditioning of the system following the approach detailed in[64]. In this way, the computational complexity of GMRES is primarily determined by the cost of matrix-vector products and the sparse multifrontal LU factorization.

Numerical results

In this section, we demonstrate the applicability of the proposed approach by considering four illustrative examples, namely, (a) a parallel plate capacitor, (b) a dielectric slab with a pair of dipole antennas, (c) a microstrip, all based on a TV dielectric slab. Finally, to show the model of a TV lumped element and its impact on EM scattering, we shall evaluate (d) the TD backscattered EM field from a small electric dipole loaded by a TV capacitor. An approximate analytical description of the latter configuration can be found in[65]. All the simulations have been carried out on a computer equipped with 384 GB of RAM and a dual-core Intel processor operating at 2.20 GHz. The PEEC method has been developed in MATLAB.

Parallel plate capacitor

In the first example, the parallel plate capacitor sketched in Fig. 6 is considered. The plates are 1 cm^2, and the thickness of the conductors and dielectric are 50 μm and 0.5 mm, respectively. The plates are made of copper with electric conductivity $\sigma = 5.8 \cdot 10^7$ S/m. The dielectric is characterized by the following TV permittivity

$$\varepsilon(t) = \varepsilon_0\varepsilon_r\left[1-\frac{1}{2}\cos(\omega_0 t)\mathrm{H}(t-T_0)+\frac{1}{2}\cos(\omega_0 t)\mathrm{H}(t-T_1)\right], \tag{34}$$

where $\varepsilon_r = 4.1, \omega_0 = 0.9 \cdot 10^9$ rad/s, the activation time is $T_0 = 1.8$ ns while the TV part of the permittivity is switched off at time $T_1 = 36.5$ ns and $\mathrm{H}(t)$ is the Heaviside step function. The TV relative permittivity is shown in Fig. 7.

A voltage source with an internal resistance $R_s = 50$ mΩ is applied to the capacitor. The voltage source has a power-exponential (PE) behavior described as[66]

$$v_s(t) = (t/t_r)^n \exp[-n(t/t_r - 1)]\mathrm{H}(t), \tag{35}$$

and depicted in Fig. 8. The voltage source is applied precisely at the center of the square parallel plate capacitor, as shown in Fig. 6. The equivalent circuit includes 10741 inductive branches (5635 dielectric-related), 2852 capacitive surfaces, and 3174 nodes. The displacement current through the capacitor has been computed using the PEEC model with constant and TV permittivity. In this last case, the quasi-static ($PEEC-QS$) and the delayed ($PEEC-DEL$) solvers have been used. For comparison purposes, the displacement current has also been computed using the FDTD method[30], a commercial tool based on the Finite Element Method (FEM) and the well-known expression for the current through a lumped capacitor, $i = \mathrm{d}q/\mathrm{d}t$ (with C_{lumped}), while

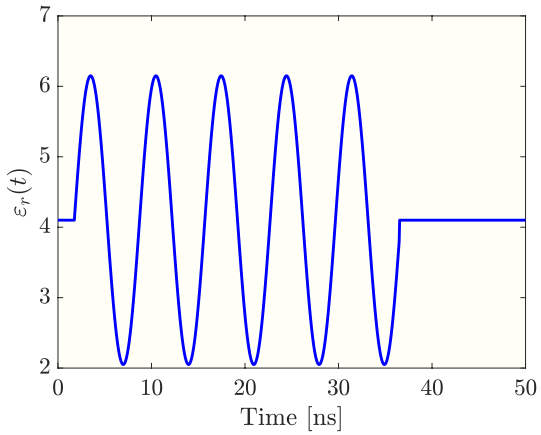

Fig. 7. TV permittivity of the parallel plate capacitor.

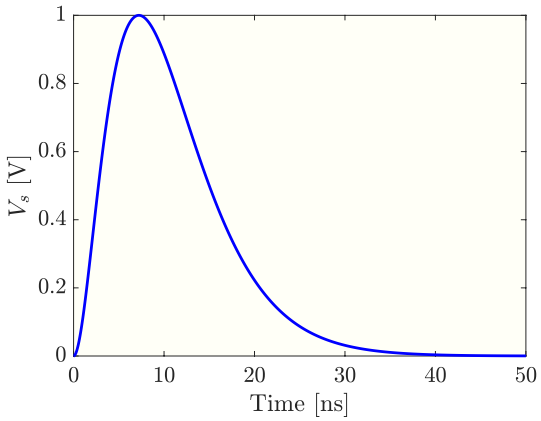

Fig. 8. Voltage source applied to the parallel plate capacitor.

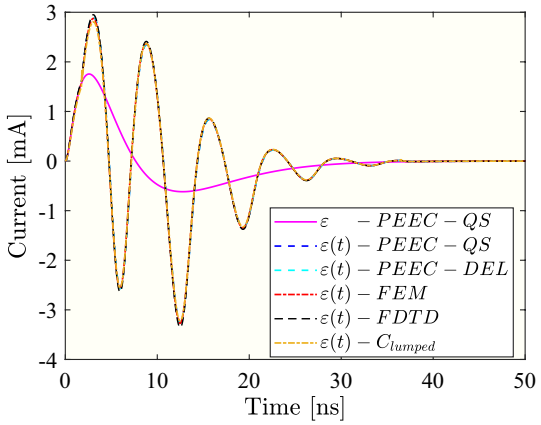

Fig. 9. Displacement current through the 1 cm^2 parallel plate capacitor.

considering the same TV permittivity. The results are shown in Fig. 9. Given the small dimensions of the plates, the four curves corresponding to the TV case almost overlap in the time interval $T_0 - T_1$.

In the second test, the size of the capacitor plates has been increased to 9 cm^2. The source, the thickness of the conductors, and the dielectric have been kept unchanged. The equivalent circuit includes 19685 inductive branches (10323 dielectric-related), 4836 capacitive surfaces, and 5766 nodes.

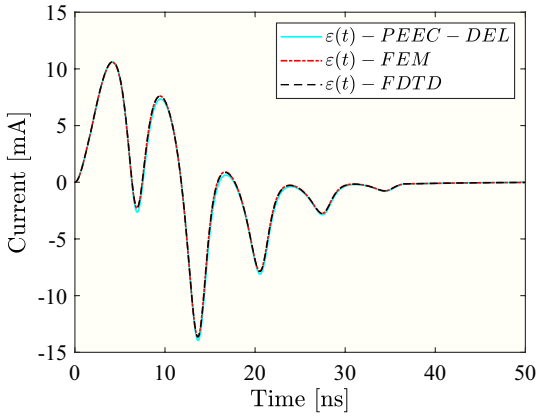

Fig. 10. Displacement current through the 9 cm^2 parallel plate capacitor.

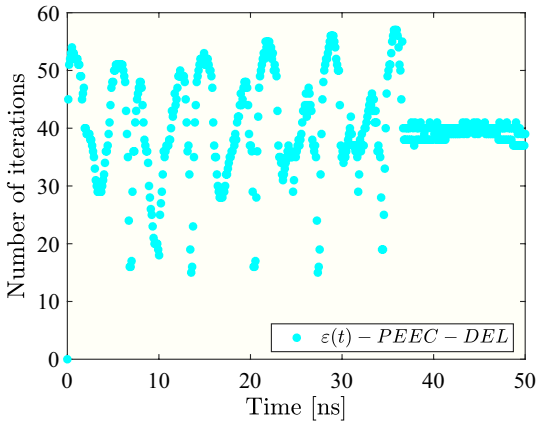

Fig. 11. Number of GMRES iterations for the 9 cm^2 parallel plate capacitor.

Number of ind. branches	Number of nodes	Number of cap. surfaces	Avg. precond. time per time sample	Avg. time per iteration	Avg. iteration number per time sample		
					GMRES tol. 1e-4	GMRES tol. 1e-5	GMRES tol. 1e-6
5120	1536	1536	120 ms	15 ms	34	57	75
10741	3174	2852	330 ms	50 ms	38	60	78
19685	5766	4836	780 ms	140 ms	40	63	79

Table 2. Performance of the GMRES iterative solver under different settings and numbers of unknowns for the 9 cm^2 parallel-plate capacitor.

For this evaluation, Fig. 10 shows the results obtained using the PEEC, FEM, and FDTD methods. A good agreement is observed across all techniques. In addition, Fig. 11 illustrates the number of GMRES iterations required by the $\varepsilon(t)$-PEEC-DEL method, using a convergence tolerance of 10^{-4}. Finally, the performance of the GMRES iterative solver, under different settings and numbers of unknowns, is reported in Table 2. As expected, decreasing the tolerance increases the number of iterations, while the average time per iteration remains relatively stable. The multifrontal sparse LU preconditioner plays a key role in ensuring this efficiency.

The average time per GMRES iteration is 0.1 s, while the average time per time sample required by the sparse multifrontal factorization (for preconditioner setup) is 0.78 s.

Dielectric Slab Excited by an Electric Dipole

In this example, a time-varying dielectric slab is considered. It occupies $\Omega = \{-L/2 \leq x \leq L/2, -W/2 \leq y \leq W/2\}$ of dimensions $\{L, W\} = \{15, 12\}$ cm (see Fig. 12). The thickness of the dielectric slab is $d = 2$ mm. Two dipoles are placed close to the slab at a distance of 1.5 mm on both sides of the slab, as shown in Fig. 12. Both dipole elements have a rectangular cross-section with a width of

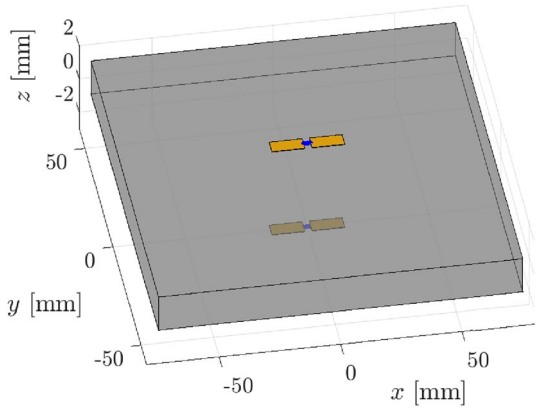

Fig. 12. Dielectric slab with a pair of transmitting and receiving dipoles.

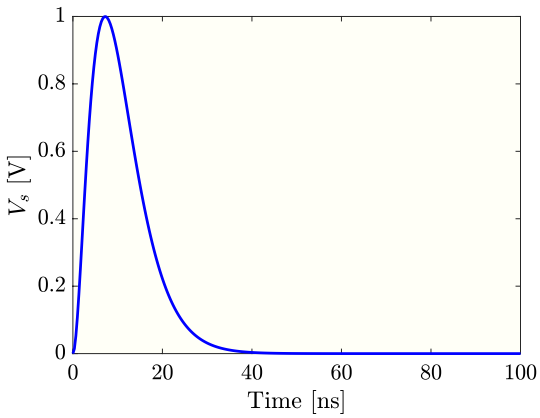

Fig. 13. Voltage source of the transmitting dipole.

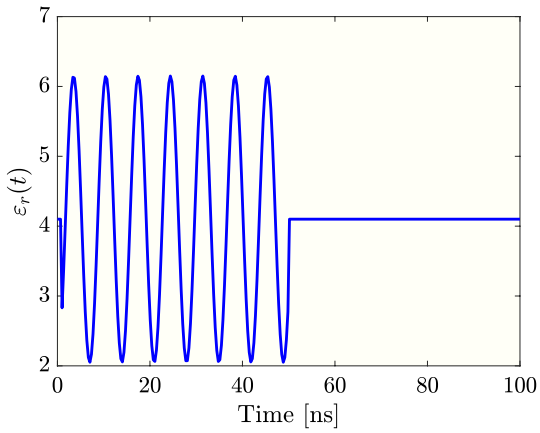

Fig. 14. TV permittivity of the dielectric slab.

$w = 4.8$ mm and a thickness of $t = 50$ μm. The length of each dipole arm is 15 mm. Both dipoles are made of copper ($\sigma = 5.8 \cdot 10^7$ S/m).

The first dipole is excited by the voltage source shown in Fig. 13, which exhibits a PE behavior with parameters $n = 2$ and $t_r = 2$ ns. Both the transmitting and receiving dipoles are terminated with 1 $k\Omega$ resistors, connected at the ports indicated by the blue lines in Fig. 12. The TV dielectric permittivity follows the profile defined in (34), with $\omega_0 = 0.9 \cdot 10^9$ rad/s, an activation time of $T_0 = 0.8$ ns, and a deactivation time of $T_1 = 50$ ns. The relative permittivity is shown in Fig. 14, with $\varepsilon_r = 4.1$; the constant permittivity value is $\varepsilon = \varepsilon_0 \varepsilon_r = 4.1\varepsilon_0$. The

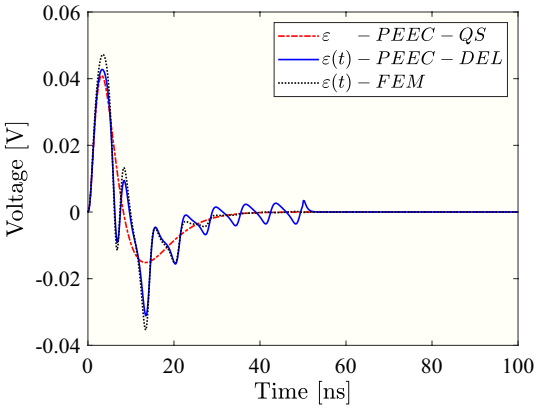

Fig. 15. TD voltage at the receiving dipole port terminated on a 1 kΩ resistance.

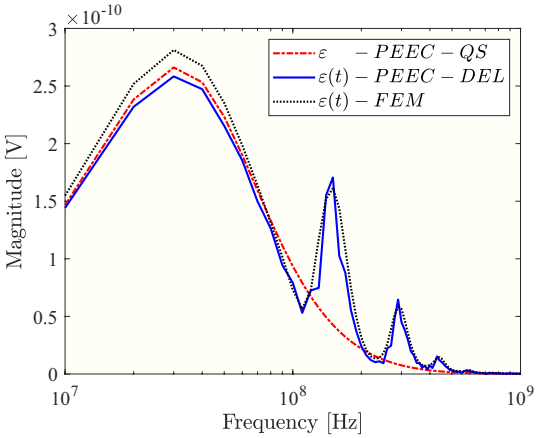

Fig. 16. Magnitude of the receiver dipole voltage port.

resulting equivalent circuit consists of 3624 inductive branches (3492 of which are related to the dielectric), 1824 capacitive surfaces, and 1512 nodes.

The voltage at the receiving dipole is shown in Fig. 15, where the effect of the sinusoidal modulation of the permittivity in the time interval $T_0 - T_1$ is visible, resulting in amplitude modulation. Furthermore, Fig. 16 reveals, via the magnitude response at the receiver dipole voltage port, distinct modulation patterns due to the time-dependent dielectric properties of the slab.

Figure 17 shows the number of GMRES iterations required by the $\varepsilon(t)$–PEEC–DEL method, with an accuracy threshold set to 10^{-4}. On average, each GMRES iteration takes 13 ms, while the sparse multifrontal factorization used for preconditioner setup requires around 30 ms per time sample.

Microstrip

The geometry of the considered microstrip is sketched in Fig. 18. It consists of a flat copper signal conductor of thickness $t = 35$ μm and width $w = 0.178$ mm, which extends longitudinally for $\ell = 3$ cm. This conductor is located on the top surface of a dielectric substrate that is $h = 0.7$ mm thick and $W = 14.534$ mm wide. A continuous ground plane, formed by a second copper layer of thickness t, is located on the underside of the substrate and shares the same width and length. The TV permittivity has been set with the following periodic modulated function:

$$\varepsilon(t) = \varepsilon_0 \varepsilon_r \left[1 + \frac{1}{2}\cos\left(2\pi f_0 t\right) \mathrm{H}(t)\right], \tag{36}$$

where $\varepsilon_r = 4.4$, and $f_0 = 37.5$ MHz. The TD voltage source is a sinusoidal signal with a frequency of $f_s = 500$ MHz and an amplitude of 1 V. Both ports are terminated with 50 Ω resistors. Figure 19 illustrates the periodically modulated permittivity profile. The equivalent circuit includes 1907 inductive branches (859 dielectric-related), 926 capacitive surfaces, and 540 nodes. The magnitude spectrum of the microstrip output voltage is shown in Fig. 20. It can be observed that the frequency dispersion induced by the time-varying permittivity is accurately reproduced. Specifically, modulation of the permittivity gives rise to spectral components at $f_1 = f_s - f_0 = 462.5$ MHz and $f_2 = f_s + f_0 = 537.5$ MHz, which are correctly identified in the results.

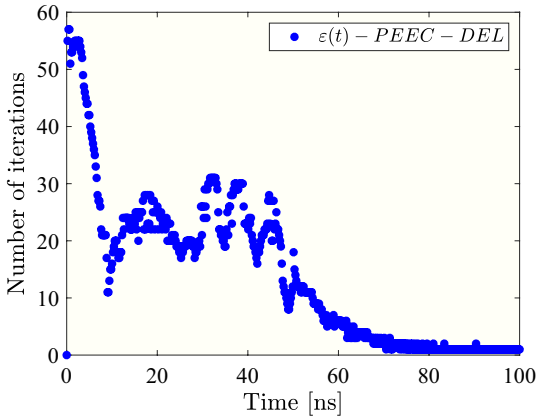

Fig. 17. Number of GMRES iterations for the dielectric slab example.

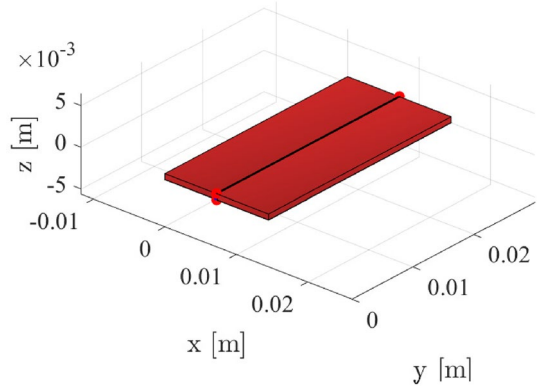

Fig. 18. Microstrip geometry.

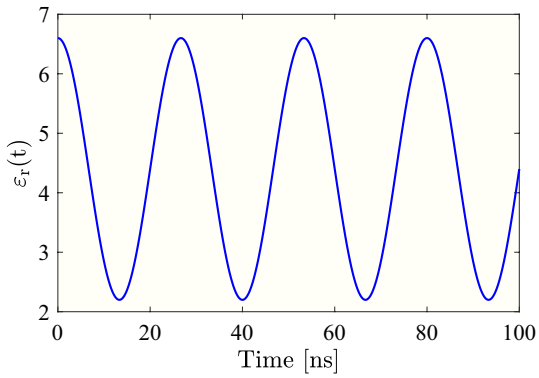

Fig. 19. TV permittivity of the microstrip substrate.

Furthermore, Table 3 reports the absolute errors at f_0 and $f_0 \pm f_s$ resulting from the comparison of the $\varepsilon(t)$ -PEEC and $\varepsilon(t)$-FDTD approaches.

For this example, the number of GMRES iterations with an accuracy threshold of 10^{-4}, is shown in Fig. 21. In this case, the average time per GMRES iteration is 4 ms, while the average time per time sample required by the sparse multifrontal factorization is 25 ms.

Dipole loaded by a TV capacitor

In this section, we evaluate the TD EM response in terms of the backscattered field from a small electric dipole loaded with a TV capacitor (see Fig. 22). An approximate analytical model of this configuration was presented in[65].

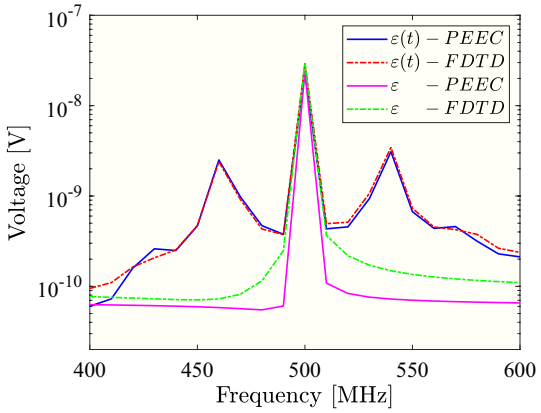

Fig. 20. Magnitude spectrum of the microstrip output voltage.

Method	$f_0 - f_s = 462.5$ MHz	$f_0 = 500$ MHz	$f_0 + f_s = 537.5$ MHz
$\varepsilon(t)$-PEEC vs. $\varepsilon(t)$-FDTD	$1.062 \cdot 10^{-10}$	$5.932 \cdot 10^{-9}$	$3.631 \cdot 10^{-10}$

Table 3. Absolute errors at f_0 and $f_0 \pm f_s$ in the magnitude spectrum of the microstrip output voltage.

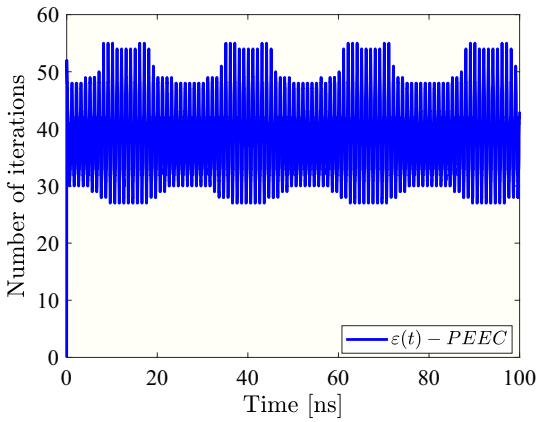

Fig. 21. Number of GMRES iterations for the microstrip example.

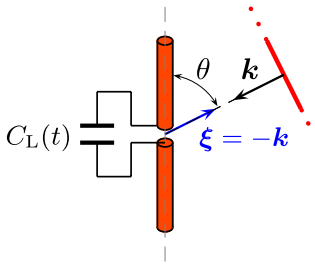

Fig. 22. Electric-dipole receiving antenna loaded by a TV lumped capacitor.

The dipole antenna is supposed to be irradiated by a uniform EM plane characterized by the PE signature defined by (35). Its pulse time width, t_{w}, is related to the pulse rise time, t_{r}, via $t_{\mathrm{w}} = t_{\mathrm{r}}\, n^{-n-1}\Gamma(n+1)\exp(n)$ [67]. For this example we set $n = 4$ and $t_{\mathrm{w}} = 50\ell/c$, where $\ell = 0.10\,\mathrm{m}$ denotes the (relatively small) dipole's length. The temporal dependence of the load capacitance is chosen according to

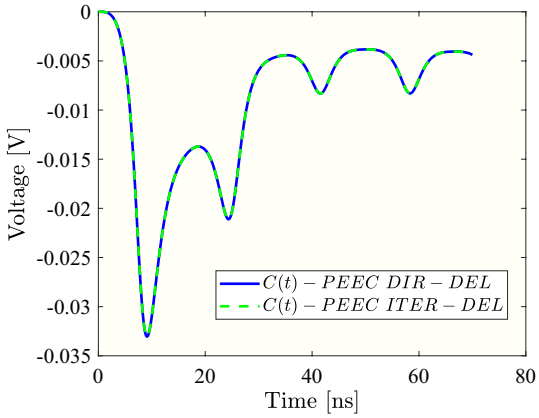

Fig. 23. Dipole port voltage induced by the incident plane wave.

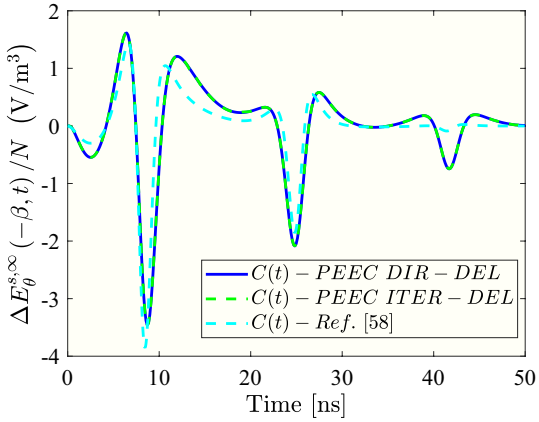

Fig. 24. The change of the EM field (with respect to the open-circuit reference) as backscattered by the wire antenna loaded by the TV capacitance (37).

$$C_{\mathrm{L}}(t) = C_0[1 + \cos(2\pi t/t_{\mathrm{w}})]\mathrm{H}(t), \tag{37}$$

with $C_0 = 1.0\,\mathrm{pF}$. The port voltage induced by the incident plane wave has been computed using two delayed PEEC solvers, one implementing a direct solver and the other an iterative one. The equivalent circuit includes 1032 inductive branches, 636 capacitive surfaces, and 450 nodes. The result is shown in Fig. 23.

Figure 24 shows the difference in the TD amplitude of the far-field backscattered electromagnetic field, compared to the response of an open-circuited antenna, as obtained both from the approximate closed-form model in[65] and from PEEC-based simulations. The comparison is shown for the observation angle $\theta = \pi/2$. The far-field TD response is scaled by the factor $N = (C_{\mathrm{a}}/4\epsilon_0)\ell^2$, where C_{a} is the dipole capacitance $C_a = \pi\epsilon_0\ell/2/\log(\ell/a)$, with $a = 1$ mm being the radius.

Conclusion

Materials with time-varying electromagnetic parameters offer the potential to overcome performance limitations inherent to their linear, time-invariant counterparts. This work presents a rigorous derivation of the contrast-source formulation for modeling TV dielectrics and lumped capacitors within the partial element equivalent circuit (PEEC) framework. The proposed formulation enables the integration of both distributed and lumped TV dielectric phenomena into PEEC by introducing time-varying capacitances and voltage-controlled current sources. These elements are naturally incorporated into the Modified Nodal Analysis (MNA) equations, resulting in a full-wave time-domain (TD) solver with an intuitive circuit-based interpretation. Furthermore, the method lends itself to straightforward integration with SPICE-like circuit simulation tools. The accuracy and effectiveness of the approach have been demonstrated through a series of illustrative examples. Notably, the method maintains computational simplicity while ensuring accurate modeling of general 3D geometries and preserving the correct representation of propagation and radiation phenomena in the presence of time-varying materials. It is worth noting that incorporating TV dielectrics does not make the PEEC model more complex, as it only requires adding extra terms to the matrices. Furthermore, even though portions of the matrices must be updated as a function of time, the computational overhead remains modest with iterative solvers.

Data availability

The datasets generated and/or analyzed during the current study are available from the corresponding author upon reasonable request.

Received: 6 August 2025; Accepted: 6 November 2025
Published online: 28 November 2025

References

1. Engheta, N. Metamaterials with high degrees of freedom: space, time, and more. *Nanophotonics* **1** (2020).
2. Morgenthaler, F. Velocity modulation of electromagnetic waves. *IRE Trans. Microw. Theory Tech.* **6**, 167–172. https://doi.org/10.1109/TMTT.1958.1124533 (1958).
3. Holberg, D. & Kunz, K. Parametric properties of fields in a slab of time-varying permittivity. *IEEE Trans. Antennas Propag.* **14**, 183–194. https://doi.org/10.1109/TAP.1966.1138637 (1966).
4. Koutserimpas, T. T. & Fleury, R. Electromagnetic waves in a time periodic medium with step-varying refractive index. *IEEE Transactions on Antennas and Propagation* **66**, 5300–5307. https://doi.org/10.1109/TAP.2018.2858200 (2018).
5. Zadeh, L. Frequency analysis of variable networks. *Proc. IRE* **38**, 291–299. https://doi.org/10.1109/JRPROC.1950.231083 (1950).
6. Pipes, L. A. Matrix analysis of linear time-varying circuits. *J. Appl. Phys.* **25**, 1179–1185 (1954).
7. Hayran, Z. & Monticone, F. Using time-varying systems to challenge fundamental limitations in electromagnetics: Overview and summary of applications. *IEEE Antennas Propag. Mag.* **65**, 29–38. https://doi.org/10.1109/MAP.2023.3236275 (2023).
8. Ptitcyn, G., Mirmoosa, M. S., Sotoodehfar, A. & Tretyakov, S. A. A tutorial on the basics of time-varying electromagnetic systems and circuits: Historic overview and basic concepts of time-modulation. *IEEE Antennas and Propagation Magazine* **65**, 10–20. https://doi.org/10.1109/MAP.2023.3261601 (2023).
9. Trinchero, R. & Stievano, I. S. F-domain analysis of linear circuits with time-varying parameters via integral equations. In *2018 IEEE International Symposium on Circuits and Systems (ISCAS)*, 1–5, https://doi.org/10.1109/ISCAS.2018.8351024 (2018).
10. Jayathurathnage, P. et al. Time-varying components for enhancing wireless transfer of power and information. *Phys. Rev. Appl.* **16**, 014017. https://doi.org/10.1103/PhysRevApplied.16.014017 (2021).
11. Horn, R., Jacobs, H., Freibergs, E. & Klohn, K. Electronic modulated beam-steerable silicon waveguide array antenna. *IEEE Transactions on Microwave Theory and Techniques* **28**, 647–653. https://doi.org/10.1109/TMTT.1980.1130133 (1980).
12. De Flaviis, F., Alexopoulos, N. & Stafsudd, O. Planar microwave integrated phase-shifter design with high purity ferroelectric material. *IEEE Transactions on Microwave Theory and Techniques* **45**, 963–969. https://doi.org/10.1109/22.588610 (1997).
13. Ramaccia, D., Sounas, D. L., Alu, A., Bilotti, F. & Toscano, A. Nonreciprocal horn antennas using angular momentum-biased metamaterial inclusions. *IEEE Transactions on Antennas and Propagation* **63**, 5593–5600. https://doi.org/10.1109/TAP.2015.2496105 (2015).
14. Fleury, R., Sounas, D. L., Sieck, C. F., Haberman, M. R. & Alu, A. Sound isolation and giant linear nonreciprocity in a compact acoustic circulator. *Science* **343**, 516–519. https://doi.org/10.1126/science.1246957 (2014).
15. Estep, N. A., Sounas, D. L., Soric, J. & Alu, A. Magnetic-free non-reciprocity and isolation based on parametrically modulated coupled-resonator loops. *Nature Physics* **10**, 923–927. https://doi.org/10.1038/nphys3134 (2014).
16. Hadad, Y., Sounas, D. L. & Alu, A. Non-reciprocal space-time gratings. In *2015 USNC-URSI Radio Science Meeting (Joint with AP-S Symposium)*, 104–104, https://doi.org/10.1109/USNC-URSI.2015.7303388 (2015).
17. Sotoodehfar, A., Mirmoosa, M. S. & Tretyakov, S. A. Waves in linear time-varying dielectric media. In *2022 16th European Conference on Antennas and Propagation (EuCAP)*, 1–5, https://doi.org/10.23919/EuCAP53622.2022.9769601 (2022).
18. Scarborough, C., Wu, Z. & Grbic, A. Efficient computation of spatially discrete traveling-wave modulated structures. *IEEE Transactions on Antennas and Propagation* **69**, 8512–8525. https://doi.org/10.1109/TAP.2021.3111337 (2021).
19. Scarborough, C. & Grbic, A. Generalized eigenvalue problem for spatially discrete traveling-wave-modulated circuit networks. *IEEE Transactions on Microwave Theory and Techniques* **71**, 511–521. https://doi.org/10.1109/TMTT.2022.3225321 (2023).
20. Rizza, C., Castaldi, G. & Galdi, V. Short-pulsed metamaterials. *Physical Review Letters* **128**, 257402. https://doi.org/10.1103/PhysRevLett.128.257402 (2022).
21. Rizza, C., Castaldi, G. & Galdi, V. *Nonlocal effects in temporal metamaterials. Nanophotonics* **11**, 1285–1295. https://doi.org/10.1515/nanoph-2021-0605 (2022).
22. Rizza, C. et al. Harnessing the natural resonances of time-varying dispersive interfaces. *Phys. Rev. Lett.* **133**, 186902. https://doi.org/10.1103/PhysRevLett.133.186902 (2024).
23. Stumpf, M., Loreto, F., Antonini, G. & Ekman, J. Pulsed wave propagation along a transmission line with time-varying wavespeed. *IEEE Microwave and Wireless Technology Letters* **33**, 963–966. https://doi.org/10.1109/LMWT.2023.3266921 (2023).
24. Stumpf, M., Antonini, G. & Ekman, J. Pulsed electromagnetic plane-wave interaction with a time-varying, thin high-dielectric layer. *IEEE Transactions on Antennas and Propagation* **71**, 6255–6259. https://doi.org/10.1109/TAP.2023.3263894 (2023).
25. Stumpf, M., Antonini, G. & Ekman, J. Transient electromagnetic plane wave scattering by a time-varying metasurface: A time-domain approach based on reciprocity. *IEEE Journal on Multiscale and Multiphysics Computational Techniques* **8**, 217–224. https://doi.org/10.1109/JMMCT.2023.3268413 (2023).
26. Štumpf, M., Antonini, G. & Ekman, J. Pulsed EM plane-wave interaction with a time-varying thin sheet. *IEEE Transactions on Antennas and Propagation* 1–1, https://doi.org/10.1109/TAP.2025.3587914 (2025).
27. de Hoop, A. T. & Lager, I. E. Closed-form analytic expressions for the pulsed-source radiated electromagnetic field in a class of media with time-varying wave speed. *Wave Motion* **51**, 418–424. https://doi.org/10.1016/j.wavemoti.2013.11.004 (2014).
28. Rao, S. M. *Time Domain Electromagnetics* (Academic Press, 1999).
29. Araneo, R. *Advanced Time Domain Modeling for Electrical Engineering* (The Institution of Engineering and Technology, 2022).
30. Yee, K. Numerical solution of initial boundary value problems involving Maxwell's equations in isotropic media. *IEEE Transactions on Antennas and Propagation* **14**, 302–307. https://doi.org/10.1109/TAP.1966.1138693 (1966).
31. Taflove and S. C. Hagness, A. *Computational Electrodynamics: the Finite-Difference Time-Domain Method* (Artech House Publishers, 2005).
32. Kaur, G. & Yilmaz, A. E. ET-AIM accelerated analysis of scattering from inhomogeneous objects with time-varying permittivity. In *2015 USNC-URSI Radio Science Meeting (Joint with AP-S Symposium)*, 113–113, https://doi.org/10.1109/USNC-URSI.2015.7303397 (2015).
33. Sayed, S. B., Ulku, H. A. & Bagci, H. An explicit MOT-TD-VIE solver for time varying media. In *2016 IEEE/ACES International Conference on Wireless Information Technology and Systems (ICWITS) and Applied Computational Electromagnetics (ACES)*, 1–2, https://doi.org/10.1109/ROPACES.2016.7465338 (2016).
34. Ruehli, A. E., Antonini, G. & Jiang, L. *Circuit Oriented Electromagnetic Modeling Using the PEEC Techniques* (Wiley-IEEE Press, 2017).
35. Antonini, G., Ruehli, A. E., Romano, D. & Loreto, F. The partial elements equivalent circuit method: The state of the art. *IEEE Transactions on Electromagnetic Compatibility* **65**, 1695–1714. https://doi.org/10.1109/TEMC.2023.3302700 (2023).
36. Romano, D., Antonini, G. & Ruehli, A. E. Time-domain partial element equivalent circuit solver including non-linear magnetic materials. *IEEE Transactions on Magnetics* **52**, 1–11. https://doi.org/10.1109/TMAG.2016.2573763 (2016).

37. Štumpf, M., Antonini, G. & Ruehli, A. E. Cagniard-DeHoop technique-based computation of retarded partial coefficients: The coplanar case. *IEEE Access* **8**, 148989–148996 (2020).
38. Štumpf, M., Loreto, F., Pettanice, G. & Antonini, G. Cagniard-DeHoop technique-based computation of retarded zero-thickness partial elements. *Engineering Analysis with Boundary Elements* **137**, 56–64 (2022).
39. Štumpf, M., Loreto, F., Pettanice, G. & Antonini, G. Partial-inductance retarded partial coefficients: Their exact computation based on the Cagniard-DeHoop technique. *Engineering Analysis with Boundary Elements* **149**, 86–91 (2023).
40. Loreto, F. et al. Modified numerical inversion of Laplace transform methods for the time-domain analysis of retarded partial elements equivalent circuit models. *IEEE Transactions on Electromagnetic Compatibility* **64**, 2179–2188. https://doi.org/10.1109/TEMC.2022.3198795 (2022).
41. Loreto, F. *Advanced Methods for the Transient Analysis of Linear Electrical Systems*. Ph.D. thesis, Università degli Studi dell'Aquila (2024).
42. Ruehli, A. & Heeb, H. Circuit models for three-dimensional geometries including dielectrics. *IEEE Transactions on Microwave Theory and Techniques* **40**, 1507–1516. https://doi.org/10.1109/22.146332 (1992).
43. Antonini, G., Ruehli, A. E. & Yang, C. PEEC modeling of dispersive and lossy dielectrics. *IEEE Transactions on Advanced Packaging* **31**, 768–782. https://doi.org/10.1109/TADVP.2008.2006659 (2008).
44. Lombardi, L., Romano, D. & Antonini, G. Partial element equivalent circuit method modeling of silicon interconnects. *IEEE Transactions on Microwave Theory and Techniques* **65**, 4794–4801. https://doi.org/10.1109/TMTT.2017.2727487 (2017).
45. Jiang, Y. & Wu, K.-L. Quasi-static surface-PEEC modeling of electromagnetic problem with finite dielectrics. *IEEE Transactions on Microwave Theory and Techniques* **67**, 565–576. https://doi.org/10.1109/TMTT.2018.2882481 (2019).
46. Jiang, Y. & Gao, R.X.-K. Compact quasi-static PEEC modeling of electromagnetic problems with finite-sized dielectrics. *IEEE Transactions on Microwave Theory and Techniques* **71**, 2373–2383. https://doi.org/10.1109/TMTT.2022.3229824 (2023).
47. Antonini, G., Romano, D., Stumpf, M. & Ekman, J. On the modeling of dielectrics with time-varying permittivity through the partial elements equivalent circuit method. In *2024 IEEE INC-USNC-URSI Radio Science Meeting (Joint with AP-S Symposium)*, 166–167, https://doi.org/10.23919/INC-USNC-URSI61303.2024.10632191 (2024).
48. Jin, J.-M. *The Finite Element Method in Electromagnetics.* 3rd edn, (Wiley-IEEE Press, Hoboken, NJ, 2014).
49. J. H. Wang, J. *Generalized Moment Method in Electromagnetics* (Wiley-Interscience, 1991).
50. Ho, C.-W., Ruehli, A. & Brennan, P. The modified nodal approach to network analysis. *IEEE Transactions on Circuits and Systems* **22**, 504–509. https://doi.org/10.1109/TCS.1975.1084079 (1975).
51. Ferranti, F. et al. Multipoint full-wave model order reduction for delayed PEEC models with large delays. *IEEE Transactions on Electromagnetic Compatibility* **53**, 959–967. https://doi.org/10.1109/TEMC.2011.2154335 (2011).
52. Ferranti, F., Antonini, G., Dhaene, T., Knockaert, L. & Ruehli, A. E. Physics-based passivity-preserving parameterized model order reduction for PEEC circuit analysis. *IEEE Transactions on Components, Packaging and Manufacturing Technology* **1**, 399–409. https://doi.org/10.1109/TCPMT.2010.2101912 (2011).
53. Ferranti, F., Antonini, G., Dhaene, T. & Knockaert, L. Passivity-preserving interpolation-based parameterized model order reduction of PEEC models based on scattered grids. *International Journal of Numerical Modelling: Electronic Networks, Devices and Fields* **24**, 478–495. https://doi.org/10.1002/jnm.793 (2011).
54. Ferranti, F. et al. Interpolation-based parameterized model order reduction of delayed systems. *IEEE Transactions on Microwave Theory and Techniques* **60**, 431–440. https://doi.org/10.1109/TMTT.2011.2181858 (2012).
55. Feng, L., Lombardi, L., Benner, P., Romano, D. & Antonini, G. Model order reduction for delayed PEEC models with guaranteed accuracy and observed stability. *IEEE Transactions on Circuits and Systems I: Regular Papers* **69**, 4177–4190. https://doi.org/10.1109/TCSI.2022.3189389 (2022).
56. Nagel, L. W. SPICE: A computer program to simulate semiconductor circuits. Electr. Res. Lab. Report ERL M520, BERK (1975).
57. Wollenberg, C. & Gurisch, A. Analysis of 3-d interconnect structures with PEEC using SPICE. *IEEE Transactions on Electromagnetic Compatibility* **41**, 412–417. https://doi.org/10.1109/15.809841 (1999).
58. Chou, C.-C. & Wu, T.-L. Direct simulation of the full-wave partial element equivalent circuit using standard SPICE [application notes]. *IEEE Microwave Magazine* **20**, 22–34. https://doi.org/10.1109/MMM.2019.2904376 (2019).
59. Gianfagna, C., Lombardi, L. & Antonini, G. Marching-on-in-time solution of delayed PEEC models of conductive and dielectric objects. *IET Microwaves, Antennas & Propagation* **13**, 42–47 (2019).
60. Pettanice, G. et al. Mutual coupling aware time-domain characterization and performance analysis of reconfigurable intelligent surfaces. *IEEE Transactions on Electromagnetic Compatibility* **65**, 1606–1620. https://doi.org/10.1109/TEMC.2023.3303619 (2023).
61. Ruehli, A., Garrett, J. & Paul, C. Circuit models for 3D structures with incident fields. In *1993 International Symposium on Electromagnetic Compatibility*, 28–32, https://doi.org/10.1109/ISEMC.1993.473786 (1993).
62. Saad, Y. *Iterative Methods for Sparse Linear Systems* (PWS Publishing Company, 1996).
63. Davis, T. A. & Duff, I. S. An unsymmetric-pattern multifrontal method for sparse LU factorization. *SIAM Journal on Matrix Analysis and Applications* **18**, 140–158 (1997).
64. Romano, D. & Antonini, G. Adaptive-cross-approximation-based acceleration of transient analysis of quasi-static partial element equivalent circuits. *IET Microwaves, Antennas and Propagation* **9**, 700–709 (2015).
65. Štumpf, M., Antonini, G., Ekman, J. & Franek, O. Pulsed EM scattering by dipoles with time-varying loads. *IEEE Trans. Antennas Propag.* **72**, 8094–8096 (2024).
66. Lager, I. E., de Hoop, A. T. & Kikkawa, T. Model pulses for performance prediction of digital microelectronic systems. *IEEE Transactions on Components, Packaging and Manufacturing Technology* **2**, 1859–1870. https://doi.org/10.1109/TCPMT.2012.2216266 (2012).
67. de Hoop, A. T., Štumpf, M. & Lager, I. E. Pulsed electromagnetic field radiation from a wide slot antenna with a dielectric layer. *IEEE Trans. Antennas Propag.* **59**, 2789–2798 (2011).

Author contributions

Conceptualization, D.R, G.P., M.S., J.E., and G.A.; methodology, D.R, G.P., M.S., I.E.L., J.E., and G.A.; software, D.R, G.P., and G.A.; validation, D.R, G.P., M.S., O.F., and G.A.; formal analysis, D.R, G.P., M.S., I.E.L., J.E., and G.A.; investigation, D.R, G.P., G.A., M.S., I.E.L., J.E., O.F., R.V., P.D.M., F.S.; writing-original draft preparation, D.R, G.P., M.S., I.E.L., J.E., R.V., P.D.M., F.S, and G.A.; supervision, D.R, G.P., M.S., I.E.L., J.E., O.F., R.V., P.D.M., F.S., and G.A. project administration, M.S., R.V., P.D.M., F.S., and G.A; funding acquisition, M.S., R.V., P.D.M., F.S., and G.A. All authors have read and agreed to the published version of the manuscript.

Funding

This work was partially supported by the Centre of Excellence on Connected, Geo-Localized, and Cyber Secure Vehicles (Ex-EMERGE), funded by the Italian Government under CIPE Resolution 70/2017, and by the Italian National Recovery and Resilience Plan (NRRP) of NextGenerationEU, partnership on "Telecommunications of the Future" (PE00000001 - program "RESTART", Structural Project 6GWINET, Cascade Call SPARKS, CUP D43C22003080001 and Focused Project INCHNET, Cascade Call ECONET, CUP J33C22002880001). The

Czech Science Foundation, under Grant No. 25-15862S, financially supported Martin Stumpf's research. Giuseppe Pettanice's contribution to this work derives from research conducted during his doctoral studies at the University of L'Aquila. This research was also partially funded by the Swedish Research Council grant no. 2024-04693_VR, which supported the contributions of Jonas Ekman and Giulio Antonini.

Declarations

Competing interests
The authors declare no competing interests.

Additional information
Correspondence and requests for materials should be addressed to G.A.

Reprints and permissions information is available at www.nature.com/reprints.

Publisher's note Springer Nature remains neutral with regard to jurisdictional claims in published maps and institutional affiliations.